Mechanics of Needle-Tissue Interaction

Roy J. Roesthuis, Youri R.J. van Veen, Alex Jahya and Sarthak Misra

MIRA - Institute of Biomedical Technology and Technical Medicine, University of Twente, The Netherlands

Abstract— When a needle is inserted into soft tissue, interaction forces are developed at the needle tip and along the needle shaft. The needle tip force is due to cutting of the tissue, and the force along the needle shaft is due to friction between needle and tissue. In this study, the friction force is determined for needles inserted into a gelatine phantom at insertion velocities of 10 mm/s and 20 mm/s. The friction force is found to be dependent on the insertion velocity. The needle tip force is calculated using the friction and insertion force, and is used as input for a mechanics-based model which predicts the amount of needle deflection. In the model, the needle is considered to be a cantilever beam supported by springs which have needle-tissue interaction stiffness (K_e). The value of the interaction stiffness is evaluated by comparing results from experiments and simulation. A mechanical needle insertion device is used to insert needles. Needle deflection during insertion is determined using a needle tip tracking algorithm. Results of this study provide insight into the mechanics of needle-tissue interaction, and can be used in studies for robotically steering needles into soft tissue.

I. INTRODUCTION

Percutaneous needle insertion is one of the most common minimally invasive medical procedures that is performed for local drug delivery, brachytherapy and biopsy. Accurate needle placement in these procedures is of importance, mainly because biopsy of an unintended tissue region can result in misdiagnosis, or in case of brachytherapy, malignant tissue is not destroyed. Inaccuracy of needle placement can be caused by several factors such as tissue inhomogeneity, tissue anisotropy, anatomical obstructions during needle insertion, and physiological processes like fluid flow and respiration.

Targeting accuracy in percutaneous needle insertion procedures can be improved by using a robot to insert needles. A number of research groups have studied the concept of robotic needle insertion [1]–[8]. Some of these groups have studied the use of thin bevel-tipped needles for needle insertion [1], [3], [4], [8]–[11]. The advantage of using thin needles with bevel tips is that they naturally bend during insertion due to assymetric distribution of forces at the needle tip (Fig. 1). This needle bending can be used to steer a needle through soft tissue. To be able to do pre-operative path planning and accurately steer a bevel-tipped needle using a robot, a model is required which predicts the amount of needle deflection during insertion into soft tissue [4].

In this study a mechanics-based model, based on the work by Misra et al. [4], is presented which predicts the amount of needle deflection. Though an analytical mechanics-based model is less complex than a finite element-based approach, it provides greater insight and framework for modeling needle-tissue interactions. The mechanics-based
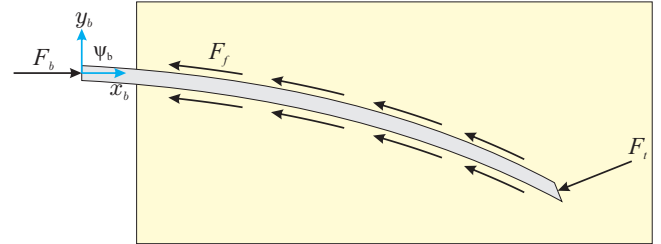

Fig. 1. As a bevel-tipped needle is inserted into a soft tissue, interaction forces are developed: F_b is the insertion force measured at the needle base, F_f is the friction force along the needle shaft and F_t is the force at the needle tip due to cutting of the tissue. The coordinate frame located at the base of the needle is indicated by ψ_b.

model requires knowledge about needle-tissue interaction forces (Fig. 1). The force along the needle shaft (F_f) is due to friction between needle and tissue, and the force at the needle tip (F_t) is a result of cutting of the tissue during insertion. Several studies have been performed to investigate the forces acting on the needle during insertion into soft tissue. Kataoka et al. [12] inserted a needle with a triangular pyramid tip into a canine prostate while measuring the insertion force. By using a needle consisting of an outer and inner part, they were able to extract the tip and the frictional force along the needle shaft from the insertion force. Okamura et al. [13] also succeeded in identifying frictional and tip forces from the insertion force measured at the base of the needle. In their experiments, needles with various bevel angles and diameters were inserted into bovine liver. They assumed that the forces at the needle tip were constant for a given tissue (i.e. independent of the internal tissue stiffness). However, their experimental result showed that the tip force increased proportionally with insertion depth due to increasing occurrences of needle collisions with internal structures in the tissue. Misra et al. [14] improved on this study by considering that the force acting on the needle tip was dependent on tissue stiffness. The goal of this work is to identify the needle-tissue interaction forces and predict needle deflection using the mechanics-based model.

The paper is organized as follows: Section II describes the needle-tissue interaction forces during insertion. In Section III, a mechanics-based model which predicts the amount of needle deflection for a bevel-tipped needle inserted into a soft tissue is derived. Section IV describes the setup used to record the forces during insertion into a gelatine phantom. It also describes the tracking algorithm used to measure the amount of needle deflection. Section V discusses the results obtained from experiments and simulation. Finally, Section VI provides conclusions and possible directions for future work.
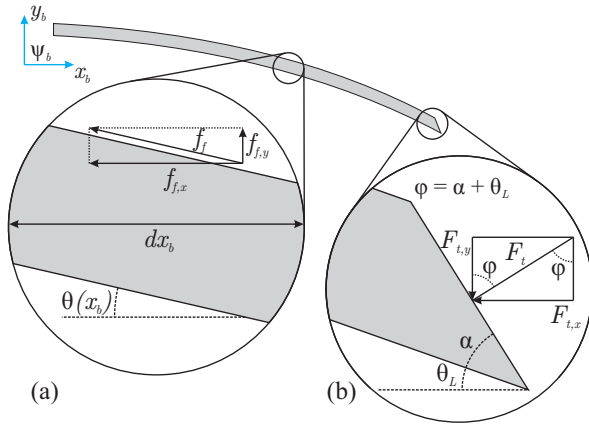
Fig. 2. Friction force along needle shaft and force at the needle tip (F_t) during insertion. (a) F_t acts normal to the needle bevel edge, $F_{t,x}$ and $F_{t,y}$ are the x_b- and y_b- component of F_t expressed in the global coordinate frame, ψ_b. $F_{t,x}$ and $F_{t,y}$ vary during insertion due to the deflection of the needle. (b) The friction force (f_f) per unit length (dx_b) along the needle shaft during insertion is decomposed to its horizontal ($f_{f,x}$) and vertical ($f_{f,y}$) components. The slope of the needle ($\theta(x_b)$) varies along the length of the needle.

II. NEEDLE-TISSUE INTERACTION FORCES

Interaction forces are developed as a bevel-tipped needle is inserted into a soft tissue (Fig.1). These interaction forces are decomposed of a friction force along the needle shaft (F_f) and a force acting normal to the needle's bevel tip (F_t). The soft tissue is considered to be viscoelastic, this means that the friction force increases as the relative velocity between needle and surrounding tissue increases. The tip force is considered to be a result from cutting of the tissue at the needle tip [13], [14].

Due to bending of the needle during insertion into a soft tissue (Fig. 2), both the friction force and tip force are composed of components acting in the x_b- and y_b-direction (expressed in ψ_b). The needle slope ($\theta(x_b)$) is defined as the angle between the needle's centre axis and the coordinate frame at the needle's base (ψ_b) observed at location x_b along the needle shaft. Using the needle slope, the components ($f_{f,x}$ and $f_{f,y}$) of the friction force (f_f) can be evaluated

$$f_{f,x} = f_f \cos\left(\theta(x_b)\right)$$
$$f_{f,y} = f_f \sin\left(\theta(x_b)\right) \tag{1}$$

where the friction force (f_f) is defined as friction per unit inserted needle length (dx_b). Total friction force in x_b- and y_b-direction ($F_{f,x}$ and $F_{f,y}$) is obtained by integrating (1) over the inserted needle length (l)

$$F_{f,x} = \int_{L-l}^{L} f_f \cos\left(\theta(x_b)\right)dx_b$$
$$F_{f,y} = \int_{L-l}^{L} f_f \sin\left(\theta(x_b)\right)dx_b \tag{2}$$

where L is the total needle length (Fig. 3).

Using the slope at the needle tip ($\theta_L = \theta(L)$) and the needle's bevel angle (α), F_t can be decomposed into two components ($F_{t,x}$ and $F_{t,y}$ in Fig. 2)

$$F_{t,x} = F_t \sin(\alpha + \theta_L)$$
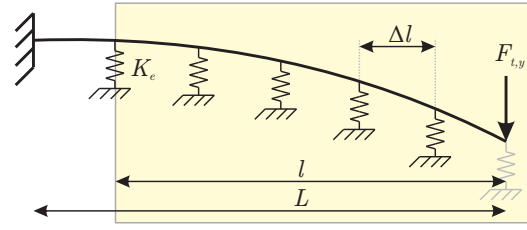$$F_{t,y} = F_t \cos(\alpha + \theta_L) \tag{3}$$

Fig. 3. The tissue elastically supports the needle as it is inserted into the tissue. This is modeled as a cantilever beam supported by a series of springs (with effective stiffness K_e) along the needle shaft and $F_{t,y}$ as the transverse tip force. The total needle length is L and the inserted needle length is l.

The insertion force (F_b) is the force required to insert a needle into a tissue (Fig. 1). At a given instant in time during insertion, the forces along the x_b-axis are in equilibrium and can be expressed as

$$F_b = -(F_{t,x} + F_{f,x}) \tag{4}$$

If the amount of friction during needle insertion is known, the needle tip force ($F_{t,x}$) can be calculated by subtracting the friction force ($F_{f,x}$) from the insertion force (F_b). Using (3) and the horizontal tip force ($F_{t,x}$), the transversal tip force ($F_{t,y}$) can be calculated. This force is used as input for a mechanics-based model which is presented in the next section.

III. MECHANICS-BASED MODEL

In this section, a mechanics-based model is developed which predicts the deflection of a bevel-tipped needle during insertion into soft tissue. In the proposed model, this is modeled as a cantilever beam supported by a series of springs which each have interaction stiffness, K_e (Fig. 3). The interaction stiffness of these springs is considered to be constant throughout the tissue. Transversal tip force ($F_{t,y}$) is taken as input and causes the needle to deflect in transversal direction. The needle will also compress in the axial direction due to $F_{t,x}$, but due to high stiffness of the needle in the axial direction this deflection is very small compared to transversal bending and is therefore neglected. The Rayleigh-Ritz method is used to evaluate the needle deflection during insertion. This method will be described in more detail in Section III-A.

The modeling of inserting a bevel-tipped needle into tissue is discretized into a series of insertion steps (Fig. 4). Each insertion step is denoted by i and the total number of insertion steps is n. In each step, the inserted needle length (l_i) is increased by Δl and the additional deflection due to transversal tip force ($F_{t,y}$) is calculated:

- Insertion step i, sub-step 1: Initially the needle is a distance l_i inside the tissue and is modeled as a cantilever beam supported by springs (configuration ⓐ) which each have stiffness K_e. In this step, transversal tip force $F_{t,y}^i$ is calculated using (3).
- Insertion step i, sub-step 2: Transversal tip force ($F_{t,y}^i$), calculated in sub-step 1, is applied and the amount of needle deflection is determined using the Rayleigh-Ritz method based on the cantilever beam model in
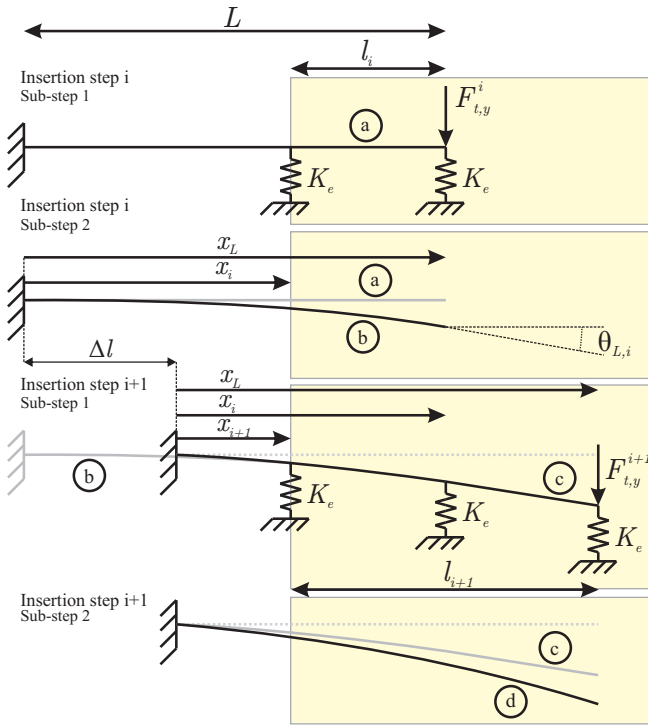
Fig. 4. Needle insertion into a tissue is modeled in a series of insertion steps. Each insertion step (i) is divided into 2 sub-steps: in the first sub-step the inserted needle distance is increased with Δl and a spring of stiffness K_e is added. In the second sub-step, the deflected needle shape is calculated by applying transversal tip force $F_{t,y}$.

sub-step 1. This results in the needle to deflect to configuration ⓑ and tip slope $\theta_{L,i}$ is calculated.

- Insertion step $i+1$, sub-step 1: Starting with configuration ⓑ, the inserted needle length is further increased with a distance Δl and this results in configuration ⓒ. An additional spring is added and tip force $F_{t,y}^{i+1}$ is calculated using (3).

- Insertion step $i+1$, sub-step 2: Transversal tip force $F_{t,y}^{i+1}$ is applied and the needle deflects to configuration ⓓ using similar steps described in sub-step 2 of step i.

The process of needle insertion continues until the final inserted needle length (l_n) is reached. The increase in inserted needle length (Δl) at each step of insertion is determined by the final inserted needle length (l_n) and the number of insertion steps (n): $\Delta l = l_n/n$.

A. Rayleigh-Ritz Method

The Rayleigh-Ritz method is a variational method in which equilibrium is established as the minimum of a potential defined by sum of the total energy and work done by the system [4]. In the expression for system potential, a displacement function is assumed which satisfies the geometric boundary conditions of the system. The deflected needle shape is evaluated by minimizing the potential of the system. The system potential of the mechanics-based model, at any step of insertion i, is given as
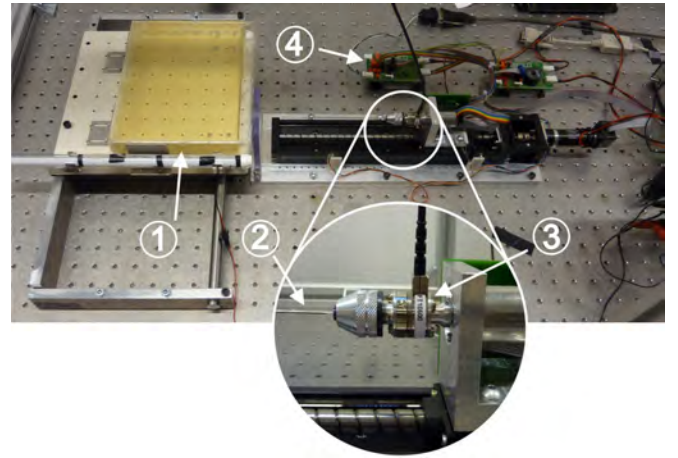
$$\Pi_i = (U_{B,i} + U_{T,i}) - W_i \tag{5}$$

Fig. 5. Two DOF setup used for inserting needles into a phantom. ① Gelatine phantom ② Needle ③ Force/torque sensor ④ Controllers

where $U_{B,i}$ and $U_{T,i}$ are the energies associated with needle bending and the needle-tissue interaction due to tissue elasticity respectively. While W_i is the work done by transversal tip load ($F_{t,y}^i$) to deform and cut tissue at the needle tip.

B. Bending Energy

When a needle is inserted into the tissue, it bends in the transversal direction. In (5), $U_{B,i}$ is the strain energy associated with transversal needle bending. At a certain step of insertion (i) for a given needle length (L), the strain energy is given by

$$U_{B,i} = \frac{E_n I}{2} \int_0^L \left(\frac{d^2 v_i}{dx^2} \right)^2 dx_b \tag{6}$$

where v_i is the deflected needle shape, E_n the needle's Young's modulus and I is the needle's second moment of inertia.

C. Energy due to Elasticity of the Tissue

The energy due to the elastic interaction between needle and tissue is determined by the difference in deflection between the current and previous needle deflection ($v_i - v_{i-1}$) at a specified spring location (x_k which equals x_i in Fig. 4). The total energy is then defined as the sum of the energies of all the individual springs along the needle shaft

$$U_{T,i} = \sum_{k=1}^n \frac{1}{2} K_e \left(v_i(x_k) - v_{i-1}(x_{k-1}) \right)^2 \tag{7}$$

D. Work done by Tip Force

The work done by the transversal force $F_{t,y}^i$ during each step of insertion depends on the difference in tip deflection between the current and previous step

$$W_i = F_{t,y}^i \left(v_i(L) - v_{i-1}(L) \right) \tag{8}$$

IV. MATERIALS AND METHODS

In this section the setup is presented which is used to insert needles into gelatine phantom. The needle tip tracking algorithm is also discussed here.
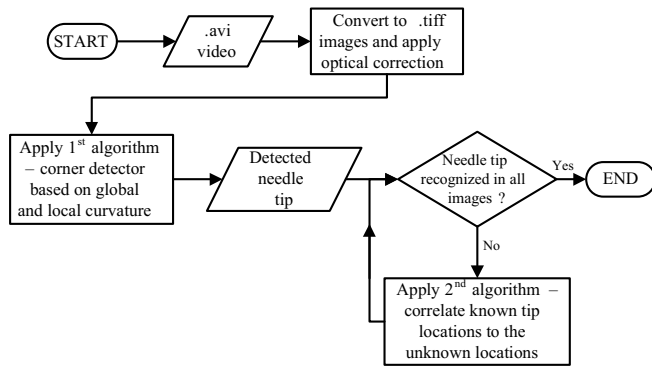
Fig. 6. Flowchart of the needle tip tracking algorithm. Input of the algorithm is a video in AVI (Audio Video Interleave) format. The tracking algorithm converts this video into series of TIFF (Tagged Image File Format) images prior to the start of the tracking procedures. This allows the needle tip to be tracked one frame at the time using the corner detector algorithm, then if necessary, by the correlation algorithm.

A. Experimental Setup

A two degree-of-freedom (DOF) needle insertion device (shown in Fig. 5) is designed for the experiments. It allows translation along and rotation about the needle's longitudinal axis. The device consists of a Misumi translation stage (type LX3010, MISUMI Group Inc. Tokyo, Japan) actuated with a Maxon Motor (type RE25, with GP26B gearhead, transmission ratio 4.4:1), and a needle rotational setup using a Maxon Motor (type ECMax22, Maxon Motor, Sachseln, Switzerland). Both motors and thus the motion are controlled using the position controller on two Elmo Whistle 2.5/60 controllers (Elmo Motion Control Ltd, Petach-Tikva, Israel). Measurement of forces/torques acting on the needle during insertion is done with a six-axis Nano17 force/torque sensor (ATI Industrial Automation, Apex, USA) located at the base of the needle. Moreover, needle insertion is recorded at 30 fps via a Sony XCD-SX90 charge-coupled device (CCD) FireWire camera (Sony Corporation, Tokyo, Japan) mounted at a height of 450 mm from the top surface of the gel. Code was written in Matlab (v7.11, Mathworks Inc., Natick, USA) to process the data retrieved from camera, Nano17 sensor and Elmo controllers.

B. Tracking of the Needle Tip

A needle tip tracking algorithm is developed based on the corner detector algorithm of Xiao et al. [15], and on the correlation algorithm of Matlab's Image Processing toolbox. The corner detector algorithm searches for the needle tip when a true corner's maximum obtuse angle is set to the needle tip bevel angle. However, due to variation in lighting intensity, it may fail to recognize the needle tip in all insertion images. Hence, the correlation algorithm is applied. It uses the knowledge of the known needle tip location
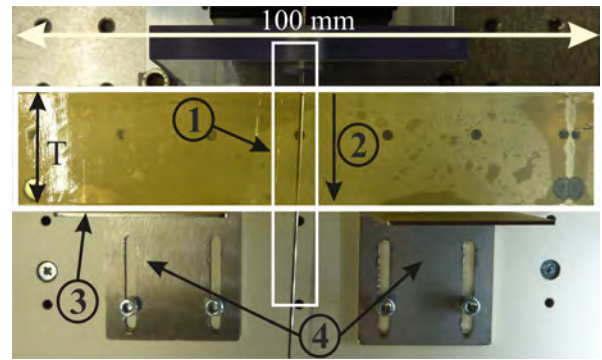

Fig. 7. Top view of the experimental setup used to measure friction force along the needle shaft. The needle ① has fully punctured a gelatine phantom. The direction of insertion is indicated by ②. A phantom ③ of 40 mm high and varying thickness T is used. ④ Two clamps were placed against the phantom to prevent it from moving during needle insertion.

and insertion speed to search for the needle tip in insertion images where the corner detector algorithm fails.

The tracking algorithm is accurate in locating the needle tip (and hence, in calculating the amount of needle tip deflection) up to 1/10 of the camera pixel resolution. The flowchart of the tracking algorithm is presented in Fig. 6.

V. RESULTS

Needle insertion experiments are performed using a solid, stainless steel needle with a bevel tip (Table I specifies the needle properties). Gelatine is used as a soft tissue to simulate the mechanical properties of human breast tissue [16]. The elasticity of the gelatine phantom was determined in a uniaxial compression test using the Anton Paar Physica MCR501 (Anton Paar GmbH, Graz, Austria) and was found to be 35 kPa. The needle is inserted at insertion velocities of 10 mm/s and 20 mm/s. These insertion velocities are representative insertion velocities during clinical percutaneous needle insertion procedures [17].

Experiments are performed to determine friction force along the needle shaft. The friction force and insertion force are used to calculate the horizontal tip force for a needle inserted to a pre-set insertion depth into the phantom. This tip force is then taken as input for the mechanics-based model to evaluate the needle-tissue interaction stiffness.

A. Friction

The friction along the needle shaft is determined by traversing the needle fully through a gelatine phantom (Fig. 7). As the needle tip has exited the gelatine phantom, the measured insertion force is taken as the friction force [4]. In Fig. 8 the measured insertion force during the experiment is shown for phantoms of different thickness (20, 30, 40

TABLE I

PROPERTIES OF NEEDLE USED IN EXPERIMENTS AND SIMULATIONS.

Parameter	Symbol	Value
Elasticity	E_n	$200 \times 10^9 \; N/m^2$
Diameter	D	$1 \; mm$
Bevel angle	α	$30°$
Length	L	$130 \; mm$

TABLE II

FRICTION PER UNIT NEEDLE LENGTH (f_f) EVALUATED FOR PHANTOMS OF DIFFERENT THICKNESS.

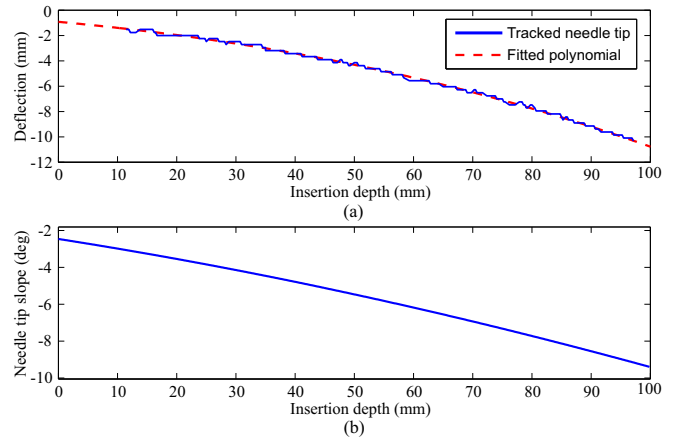| Phantom (mm)	$f_f(N/mm)$ 10 mm/s	20 mm/s
20	0.0284	0.0329
30	0.0230	0.0322
40	0.0262	0.0344
50	0.0285	0.0359
Average	0.0265	0.0339

Fig. 9. (a) Shown are the tracked needle tip during insertion at 10 mm/s and a third-order polynomial (v_{pol}) fitted to this deflection data (b) Slope of the needle tip.

Using the needle tip slope (Fig. 9(b)) and the average friction per unit needle length (f_f in Table II), the horizontal component of friction ($F_{f,x}$) can be calculated for any inserted needle length (l_i)

$$F_{f,x} = \int_0^{l_i} f_f \cos\left(\theta(x_b)\right) dx_b \qquad (10)$$

The horizontal tip force ($F_{t,x}$) is calculated by subtracting the calculated friction force from the insertion force (4). It can be seen (Fig. 10) that tip force is increasing in magnitude in the beginning of the insertion procedure. As insertion continues, it is expected that tip force ($F_{t,x}$) increases due to increase in needle tip slope (3) as the needle bends. However, it can be seen that tip force remains fairly constant and even decreases at some point for insertion at 20 mm/s. Air pockets in the phantom can cause these changes in the measured insertion force. Comparing the magnitude of the tip force in Fig. 10(a) with Fig. 10(b), it appears that there is no apparent difference in tip force for the 10 mm/s and 20 mm/s insertion velocities. This observation concurs with the fact that the transversal tip force causes needle bending, since there was no appreciable difference in the observed amount of deflection for insertion at 10 mm/s and 20 mm/s.

C. Simulated versus Experimental Needle Deflection

The results of the simulated needle deflection, using the mechanics-based model described in Section III, are now presented and compared with the experimental results.

In order to determine the needle shape using the Rayleigh-Ritz method, an assumed displacement function has to be defined which satisfies the geometric boundary conditions of the system. The assumed displacement function is defined by three third-order polynomials ($v_{a,i}$, $v_{b,i}$ and $v_{c,i}$). Each polynomial describes the deflection of the needle for a different part of the needle

$$v_i = \begin{cases} v_{a,i} & 0 \le x_b \le L/3 \\ v_{b,i} & L/3 \le x_b \le 2L/3 \\ v_{c,i} & 2L/3 \le x_b \le L \end{cases} \qquad (11)$$

Fig. 8. Insertion force for a needle inserted through gelatine phantoms of varying thickness (20, 30, 40 and 50 mm) and for a needle inserted compeletely into a gelatine phantom (Full insertion). The experiments were performed at two different insertion velocities: (a) 10 mm/s and (b) 20 mm/s. The arrows indicate the different events during insertion for the 50 mm thick phantom: ① As the needle initially punctures the phantom, a small increase in insertion force is measured. An increase in insertion force is seen as the needle traverses through the phantom. ② The needle tip exits the tissue and this results in a drop in insertion force. ③ After the needle tip has fully traversed through the phantom, the insertion force reaches a constant value. This constant value is the horizontal friction force ($F_{f,x}$).

and 50 mm). Using (2) and the measured friction ($F_{f,x}$), the friction force per unit needle length (f_f) is calculated for each of the phantoms (Table II). Friction force is determined by taking the average friction force of the different phantoms. As expected, friction force per unit needle length is higher for insertion at 20 mm/s.

B. Needle Insertion

The needle is inserted 100 mm into the gelatine phantom. After insertion has finished, the tracking algorithm is run on the recorded video to determine the amount of needle deflection. No appreciable difference in the amount of needle deflection is observed between insertion at 10 mm/s and 20 mm/s. Therefore, only the needle deflection for the insertion performed at 10 mm/s is shown in Fig. 9(a).

Since the tracking algorithm does not give a smooth needle shape (Fig. 9(a)), a third-order polynomial (v_{pol}) is fitted to the tracked needle tip data. By taking the derivative of the polynomial to the needle's length (x_b), the slope of the needle tip is calculated

$$\theta(x_b) = \tan^{-1}\left(\frac{dv_{pol}}{dx_b}\right) \approx \frac{dv_{pol}}{dx_b} \qquad (9)$$
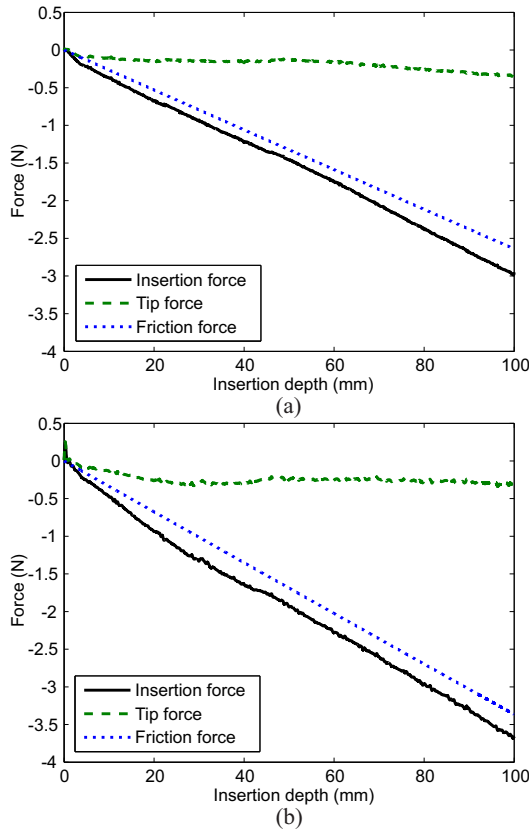
Fig. 10. The horizontal tip force ($F_{t,x}$) is calculated by subtracting the horizontal component of the friction force ($F_{f,x}$) from the insertion force (F_b) for insertion at (a) 10 mm/s and (b) 20 mm/s.

where

$$v_{a,i} = a_{0,i} + a_{1,i}x_b + a_{2,i}x_b{}^2 + a_{3,i}x_b{}^3$$
$$v_{b,i} = b_{0,i} + b_{1,i}x_b + b_{2,i}x_b{}^2 + b_{3,i}x_b{}^3 \qquad (12)$$
$$v_{c,i} = c_{0,i} + c_{1,i}x_b + c_{2,i}x_b{}^2 + c_{3,i}x_b{}^3$$

The advantage of having multiple polynomials along the needle is that the actual deflection can be approximated more precisely. It is found that increasing the polynomial degree or number of polynomials beyond three did not influence needle deflection results.

The displacement function (11) should satisfy the geometric boundary conditions of the system. The needle is fixed at the base ($x_b = 0$), causing needle rotation (dv_i/dx_b) and displacement ($v_i(x_b)$) to be constrained

$$v_i(0) = \theta(0) = \frac{dv_i}{dx_b}\big|_{x_b=0} = 0 \qquad (13)$$

The displacement function (11) also has to satisfy continuitiy conditions at the boundaries ($x_b = L/3, 2L/3$) between each of the polynomials. Applying continuity conditions for needle deflection (12) gives

$$\begin{aligned} v_{a,i}(L/3) &= v_{b,i}(L/3) \\ v_{b,i}(2L/3) &= v_{c,i}(2L/3) \end{aligned} \qquad (14)$$

and applying continuity conditions for needle slope gives

$$\begin{aligned} \frac{dv_{a,i}}{dx_b} &= \frac{dv_{b,i}}{dx_b}\big|_{x_b=L/3} \\ \frac{dv_{b,i}}{dx_b} &= \frac{dv_{c,i}}{dx_b}\big|_{x_b=2L/3} \end{aligned} \qquad (15)$$
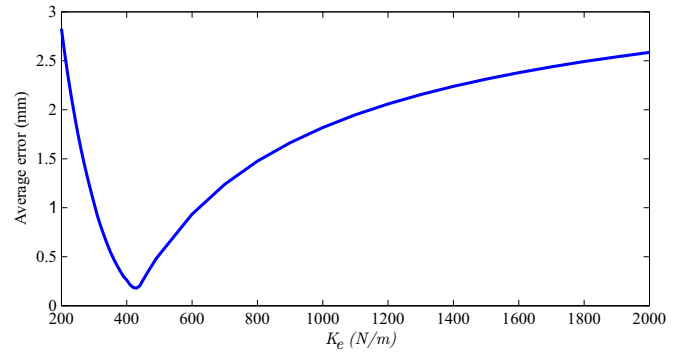

Fig. 11. Comparing the average error between simulated and experimental deflection for different values of the interaction stiffness (K_e).

Equations (13), (14) and (15) are solved for coefficients $a_{k,i}$, $b_{k,i}$ and $c_{k,i}$ for $k = 0, 1$. The remaining coefficients $a_{k,i}$, $b_{k,i}$ and $c_{k,i}$ for $k = 2, 3$ are evaluated in each step of insertion (i) by minimizing the system potential defined in (5)

$$\frac{\partial \Pi}{\partial a_{k,i}} = \frac{\partial \Pi}{\partial b_{k,i}} = \frac{\partial \Pi}{\partial c_{k,i}} = 0 \qquad (16)$$

The deflected needle shape (11) is found by substituting the coefficients back into the polynomials (12).

The mechanics-based model requires the transversal tip force ($F_{t,y}$) as input in order to determine needle deflection. The transversal tip force ($F_{t,y}$) can be calculated if the tip force normal to the bevel face (F_t) is known (3). Normal tip force (F_t) can be calculated with horizontal tip force ($F_{t,x}$) and needle tip slope (θ_L)

$$F_t = \frac{F_{t,x}}{\sin(\alpha + \theta_L)} \qquad (17)$$

In Fig. 10 it is shown that horizontal tip force ($F_{t,x}$) equals 0.3 N for both insertion at 10 mm/s and 20 mm/s as the needle is fully inserted. The corresponding needle tip slope (θ_L) at this point of insertion is found to be 9.2° (Fig. 9b). Using these numbers and a bevel angle (α) of 30°, a tip force of 0.47 N is calculated with (17). With F_t known, transversal tip force ($F_{t,y}$) can now be calculated using needle tip slope ($\theta_{L,i}$) during insertion

$$F_{t,y} = F_t \cos(\alpha + \theta_{L,i}) \qquad (18)$$

The mechanics-based model (described in Section III) is evaluated for a range of values for needle-tissue interaction stiffness (K_e). The optimal value for the interaction stiffness is found by minimizing the error between simulated and experimental deflection. The average error (in mm) is defined as the integral of the absolute error divided by the inserted needle length (l)

$$\text{average error} = \frac{1}{l} \int_{L-l}^{L} |v_{exp}(x_b) - v_{sim}(x_b)| dx_b \qquad (19)$$

For low values of the interaction stiffness ($K_e = 200$ N/m), needle deflection is large. This results in a large error (2.7 mm) between simulation and experiment (Fig. 11). Choosing a large value ($K_e > 2000$ N/m) for the interaction stiffness results in very little needle deflection, again causing a large error. The optimal value for the interaction stiffness is
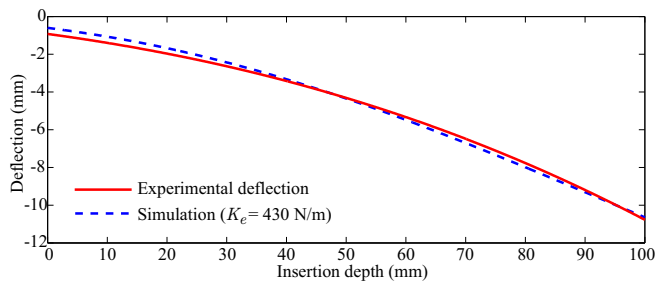
Fig. 12. Experimental needle deflection compared with simulated needle deflection using the mechanics-based model. The model was executed using the optimal stiffness value of 430 N/m.

found to be 430 N/m, the corresponding error is 0.179 mm. In Fig. 12, the simulated needle deflection is compared with the experimental needle deflection. The maximum error (0.32 mm) occurs in the beginning of the insertion (0-30 mm). A probable cause for this large error is that interaction stiffness near the edge of the phantom is different from the center. This was not taken into acount since the interaction stiffness was considered to be constant throughout the phantom.

VI. CONCLUSIONS AND FUTURE WORK

In this study, needle-tissue interaction forces were identified for a bevel-tipped needle inserted into a gelatine phantom. The friction force, expressed in friction per unit needle length, was determined in a series of experiments and was found to be 0.0265 N/mm for a needle inserted at 10 mm/s and 0.0339 N/mm for a needle inserted at 20 mm/s. The tip force was extracted from the insertion force using the friction force. No appreciable difference in needle tip force was observed between a needle inserted at 10 mm/s and 20 mm/s. Using a mechanics-based model, simulated needle deflection was compared to experimental needle deflection to evaluate the needle-tissue interaction stiffness (K_e). It was found that an interaction stiffness of 430 N/m minimizes the difference between simulated and experimental needle deflection.

In this study it was assumed that the interaction stiffness is constant at each location along the needle shaft. In future work, the interaction stiffness will be considered a function of location in the phantom. Experiments were done using homogeneous gelatine phantoms. Experiments will be done using gels of varying elasticity to relate interaction stiffness to phantom imhomogeneity. The interaction stiffness of 430 N/m is related to the needle-tissue combination used in the experiments in this study. For purposes of pre-operative path planning, knowledge is required about the relationship between interaction stiffness, and needle and tissue parameters to be able to predict needle deflection. Therefore, relationships between the interaction stiffness, and constitutive needle and tissue parameters, such as tissue elasticity and needle geometry, needs to be derived. When considering future patient studies, ultrasound elastography can provide tissue elasticity such that needle deflection can be predicted using the mechanics-based model.

The mechanics-based model presented here can be used to study needle steering into soft tissue. Knowledge about the deflection is required to accurately plan the needle path, and provide appropriate control inputs to robotically steer the needle.

REFERENCES

[1] R. J. Webster III, J. S. Kim, N. J. Cowan, G. S. Chirikjian, and A. M. Okamura, "Nonholonomic modeling of needle steering," *Int'l. J. Robotics Research*, vol. 25, no. 5-6, pp. 509–525, 2006.

[2] D. Glozman and M. Shoham, "Image-guided robotic flexible needle steering," *IEEE Transactions on Robotics*, vol. 23, no. 3, pp. 459–467, 2007.

[3] N. Abolhassani and R. V. Patel, "Deflection of a flexible needle during insertion into soft tissue," in *Proc. IEEE Int'l. Conf. Engineering in Medicine and Biology Society (EMBS)*, (New York City, USA), pp. 3858–3861, August-September 2006.

[4] S. Misra, K. B. Reed, B. W. Schafer, K. T. Ramesh, and A. M. Okamura, "Mechanics of flexible needles robotically steered through soft tissue," *Int'l. J. Robotics Research*, vol. 29, no. 13, pp. 1640–1660, 2010.

[5] N. Abolhassani, R. Patel, and M. Moallem, "Needle insertion into soft tissue: A survey," *Medical Engineering and Physics*, vol. 29, no. 4, pp. 413–431, 2007.

[6] H. Elhawary, Z. Tse, M. Rea, A. Zivanovic, B. Davies, C. Besant, N. de Souza, D. McRobbie, I. Young, and M. Lamperth, "Robotic system for transrectal biopsy of the prostate: Real-time guidance under mri," *IEEE Engineering in Medicine and Biology Magazine*, vol. 29, pp. 78–86, march-april 2010.

[7] J. J. Fütterer, S. Misra, and K. J. Macura, "Mri of the prostate: potential role of robots," *Imaging in Medicine*, vol. 2, no. 5, pp. 583–592, 2010.

[8] J. A. Engh, G. Podnar, S. Y. Khoo, and C. N. Riviere, "Flexible needle steering system for percutaneous access to deep zones of the brain," in *Proc. IEEE 32nd Annual Northeast Bioengineering Conf*, pp. 103–104, 2006.

[9] S. Misra, K. B. Reed, A. S. Douglas, K. T. Ramesh, and A. M. Okamura, "Needle-tissue interaction forces for bevel-tip steerable needles," in *Proc. IEEE Int'l. Conf. Engineering in Medicine and Biology Society (EMBS)*, (Scottsdale, AZ, USA), pp. 224–231, August 2008.

[10] R. Alterovitz, K. Goldberg, and A. M. Okamura, "Planning for steerable bevel-tip needle insertion through 2d soft tissue with obstacles," in *Proc. Int'l. Conf. Robotics and Automation (ICRA)*, (Barcelona, Spain), pp. 1640–1645, April 2005.

[11] S. Y. Ko, B. L. Davies, and F. Rodriguez y Baena, "Two-dimensional needle steering with a "programmable bevel" inspired by nature: Modeling preliminaries," in *Proc. IEEE/RSJ Int Intelligent Robots and Systems (IROS) Conf*, pp. 2319–2324, 2010.

[12] H. Kataoka, T. Washio, K. Chinzei, K. Mizuhara, C. Simone, and A. M. Okamura, "Measurement of the tip and friction force acting on a needle during penetration," in *Proc. of the 5th Int'l. Conf. on Medical Image Computing and Computer-Assisted Intervention-Part I*, MICCAI '02, (London, UK), pp. 216–223, Springer-Verlag, September 2002.

[13] A. M. Okamura, C. Simone, and M. D. O'Leary, "Force modeling for needle insertion into soft tissue," *IEEE Transactions on Biomedical Engineering*, vol. 51, no. 10, pp. 1707–1716, 2004.

[14] S. Misra, K. B. Reed, K. T. Ramesh, and A. M. Okamura, "Observations of needle-tissue interactions," in *Proc. IEEE Int'l. Conf. Engineering in Medicine and Biology Society (EMBS)*, (Minneapolis, USA), pp. 262–265, 2009.

[15] C. H. Xiao and H. Yung, "Corner detector based on global and local curvature properties," *Optical Engineering*, vol. 47, no. 5, pp. 1–12, 2008.

[16] A. Gefen and B. Dilmoney, "Mechanics of the normal woman's breast," *Technology and Health Care*, vol. 15, no. 4, pp. 259–271, 2007.

[17] N. Abolhassani, R. Patel, and M. Moallem, "Control of soft tissue deformation during robotic needle insertion," *Minimally Invasive Therapy and Allied Technologies*, vol. 15, no. 3, pp. 165–176, 2006.